Available online at www.sciencedirect.com

ScienceDirect

IFAC Papers Online CONFERENCE PAPER ARCHIVE

IFAC-PapersOnLine 48-15 (2015) 411–418

Nonlinear Model Predictive Control of an Organic Rankine Cycle for Exhaust Waste Heat Recovery in Automotive Engines

Marco Crialesi Esposito*, Nicola Pompini*, Agostino Gambarotta*
Vetrivel Chandrasekaran, Junqiang Zhou**, Marcello Canova****

**Industrial Engineering Department, University of Parma ITALY*
***Center for Automotive Research, The Ohio State University USA*

Abstract: Energy recovery from exhaust gas waste heat can be regarded as an effective way to improve the energy efficiency of automotive powertrains, thus reducing CO_2 emissions. The application of Organic Rankine Cycles (ORCs) to waste heat recovery is a solution that couples effectiveness and reasonably low technological risks. On the other hand, ORC plants are rather complex to design, integrate and control, due to the presence of heat exchangers operating with phase changing fluid, and several control devices to regulate the thermodynamic states of the systems. Furthermore, the power output and efficiency of ORC systems are extremely sensitive to the operating conditions, requiring precise control of the evaporator pressure and superheat temperature.

This paper presents an optimization and control design study for an Organic Rankine Cycle plant for automotive engine waste heat recovery. The analysis has been developed using a detailed Moving Boundary Model that predicts mass and energy flows through the heat exchangers, valves, pumps and expander, as well as the system performance. Starting from the model results, a nonlinear model predictive controller is designed to optimize the transient response of the ORC system. Simulation results for an acceleration-deceleration test illustrate the benefits of the proposed control strategy.

Keywords: Modeling, Optimization, Optimal Control, Waste Heat Recovery, Organic Rankine Cycles.

1. INTRODUCTION

As regulations on CO_2 emissions for passenger cars and light duty trucks are becoming increasingly stringent and the fuel prices keep rising, the development of cutting edge technologies for vehicle fuel economy improvement is a major area of interest for automotive manufacturers. Among the technologies currently under development, Organic Rankine Cycle (ORC) plants can be regarded as an effective solution for automotive waste heat recovery (Chiara and Canova, 2013; Wang et al, 2011). Several contributions have been recently made for vehicle applications, with reductions in fuel consumption ranging from 5 to 10% (depending on the system and the driving cycle) up to 15% in highway conditions have been documented, see for instance (Briggs et al, 2010; Edwards et al, 2010; Seher et al, 2012; Lang et al, 2014; Hosain and Bari, 2014).

Nevertheless, very few contributions in the field of control and optimization of ORC systems have been proposed in recent years. For instance, (Peralez et al., 2013) used a Moving Boundary Model to generate a set of feed-forward references for the control and to tune a PID tracking controller. (Feru et al., 2014) used a finite volume model for the ORC plant to linearize the system and synthesize a model predictive controller to track a set point in the expander inlet quality, to ensure safe operating conditions and high power output. It is clear that developing optimization and control algorithms for Organic Rankine Cycles operating in transient conditions poses significant challenges, due to the complexity of the plant dynamics, and the presence of multiple constraints and limitations in the inputs and outputs.

This paper proposes a nonlinear model predictive control approach for the transient optimization of an Organic Rankine Cycle for exhaust gas waste heat recovery in an automotive IC engine. A detailed model was developed for simulation of the ORC plant, and calibrated using components data from various suppliers. The model, which adopts a switching Moving Boundary Method for the characterization of the transient behaviour of the heat exchangers, is able to predict the mass and energy flows in the key system components, leading to the definition of the system operating conditions and overall performance. Then a constrained optimal control problem is formulated to maximize the system performance and ensure operations within the physical limits of the components. Particle Swarm Optimization (PSO) is applied to solve the receding horizon optimization problem in the NMPC framework (Sandou and Olaru 2009, Mercieca and Fabri 2012).

Verification was conducted on a transient test corresponding to an acceleration-deceleration manoeuvre. The solution generated by the MPC algorithm is compared against a feed-forward controller based upon a quasi-static optimization, a typical process adopted for the control of ORC plants.

2. SYSTEM DESCRIPTION

This study focuses on an Organic Rankine Cycle system for exhaust waste heat recovery in a turbocharged spark-ignition (SI) engine for passenger car applications. The system

10.1016/j.ifacol.2015.10.059

operates with R245fa as the working fluid, and its layout is illustrated in Fig. 1. A positive displacement pump controls flow of the refrigerant through a heat exchanger where the fluid receives heat from a flow of exhausts coming from the engine. A bypass valve is used to control the exhaust flow. The refrigerant then flows through an expander, generating mechanical work, and finally through a condenser.

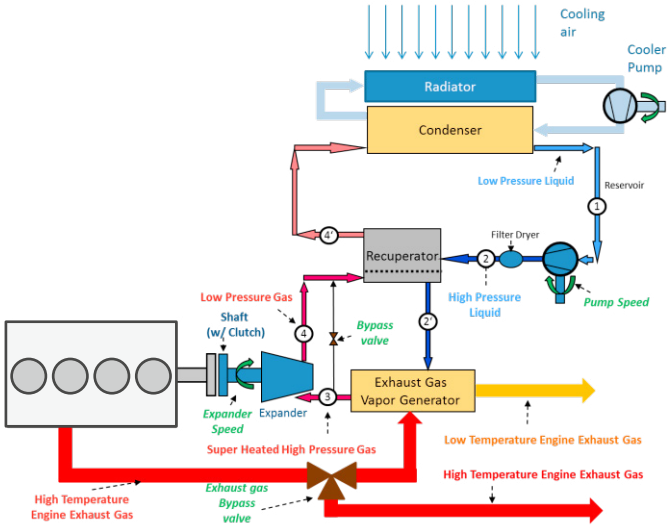

Fig. 1. Schematic of the ORC System Layout.

The ORC system is designed to operate at best efficiency at highway driving conditions, where the evaporator is intended to generate superheated vapour at the outlet. On the other hand, it may occur that during fast transients (e.g. cut-off conditions, low load...), the exhaust gas heat is insufficient to fully vaporize the refrigerant, thereby resulting into two phase vapour at the evaporator outlet. This condition, which may result in inefficient performance or unsafe behaviour of the expander, could be avoided by inserting a liquid phase separator at the evaporator outlet, bypassing the liquid directly to the condenser.

For the application considered in this study, the ORC system is directly coupled to the engine with a 1:1 gear ratio. This solution allows a more efficient use of the expander power output, without the needs of auxiliary components (such as CVTs or variable slip clutches), leading to a cost reduction.

A low-temperature cooling circuit must be used to reject the heat at the condenser. The coolant flow rate can be controlled with an electric pump. Cooling water is assumed to enter the condenser with a temperature of approximately 298K: despite the fact that this temperature could be difficult to be maintained in some conditions, the change of condensing temperature set point has no effect on the proposed methodology.

3. ORC SYSTEM MODEL

To facilitate the optimization and control design for the ORC system, a fast-running physics-based mathematical model has been developed for simulating the transient behaviour of the ORC system. The model accounts for the key components of the system, with reference to the layout sketched in Fig. 1. Thermodynamic properties of the working fluid were obtained from the NIST database, as functions of pressure and enthalpy (Lemmon et al., 2007).

3.1 Pump and Expander

The pump and expander models are based on a quasi-steady, black-box approach, (Canova et al., 2014), (Briggs et al., 2010), and calibrated using steady-state performance maps.

The expander is a positive-displacement machine whose performance parameters (volumetric efficiency η_v and isentropic efficiency η_s) are defined as:

$$\eta_v = \frac{\dot{m}_{\exp}}{\rho_{in} V_d \omega_{\exp}}; \quad \eta_s = \frac{h_{in} - h_{out}}{h_{in} - h_{out,s}} \tag{1}$$

where $\dot{m}_{\exp}$ denotes the mass flow rate of refrigerant through the expander, V_d is the expander displacement, ρ and h are the refrigerant density and enthalpy. The isentropic and volumetric efficiency are modelled through an empirical model calibrated directly on the performance data provided by the supplier.

A similar approach is used for the pump model, for which the volumetric efficiency is given by:

$$\eta_v = \frac{\dot{m}_{pump}}{\rho_{in} V_d \omega_{pump}} \tag{2}$$

Due to the very limited enthalpy changes across the pump, the pump isentropic efficiency is assumed constant.

3.2 Recuperator

The recuperator model is based upon the *ε-NTU* method. Due to the high heat transfer coefficients, the heat exchanger is characterized by a rapid response to variations in the flow rates or inlet thermodynamic conditions. For this reason, a quasi-static approach can be used to model the heat transfer (Agarwal et al., 2012). The effectiveness is evaluated as a function of the flow rate and temperatures of the incoming fluids. A dynamic model for the outlet temperature estimation is based on energy balance equation:

$$MC \frac{dT_{out}}{dt} = \dot{m} c_p \left(T_{in} - T_{out}\right) + \dot{Q}_{in} \tag{3}$$

where M is the mass of fluid contained in the heat exchanger and $\dot{Q}_{in}$ is the heat absorbed (positive) or rejected (negative) by the fluid. Equation (3) is applied to both the hot side and cold side of the recuperator.

3.3 Expander bypass

The expander bypass is modelled as an ideal valve that automatically removes any liquid flow at the outlet of the evaporator, and routes it directly to the condenser.

3.4 Condenser and Evaporator

A physically-based modelling approach, namely the Switching Moving Boundary Modelling (MBM) technique, is used to accurately simulate the evaporator and condenser behaviour (Jensen, 2003; McKinley et al., 2008; Li et al., 2010). The model equations are obtained by integrating the mass and energy balance over a number of control volumes, which discretize the length of the heat exchanger, and assuming that the working fluid thermodynamic properties are homogeneously distributed within each control volume. A lumped-parameter approximation of the fluid properties is therefore possible in each control volume due to the uniform distribution of the thermodynamic states, as illustrated in Fig. 2. The positions of the boundaries between adjacent Control Volumes become additional unknowns for the model.

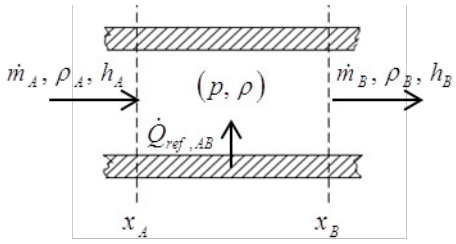

Fig. 2. Schematic of a Control Volume for Moving Boundary Heat Exchanger Model.

Mass and energy conservation equations take the form:

$$A\frac{d}{dt}\int_{x_A}^{x_B}\rho dz + A\rho_A\frac{dx_A}{dt} - A\rho_B\frac{dx_B}{dt} = \dot{m}_A - \dot{m}_B \tag{4}$$

$$A\frac{d}{dt}\int_{x_A}^{x_B}\rho h\,dz - A\left(x_B - x_A\right)\frac{dp}{dt} + A\rho_A h_A\frac{dx_A}{dt} - A\rho_B h_B\frac{dx_B}{dt} = \\ = \dot{m}_A h_A - \dot{m}_B h_B + \dot{Q}_{AB}$$

where A is the cross sectional area and x_A, x_B represent the left and right positions of the boundary for the control volume. A schematic overview of the evaporator model, under the assumption that all three zones are present, is shown in Fig. 3. During nominal operations, the working fluid enters as Subcooled (SC) liquid, then transitions through a Two Phase (TP) fluid and finally exits as Superheated (SH) vapour.

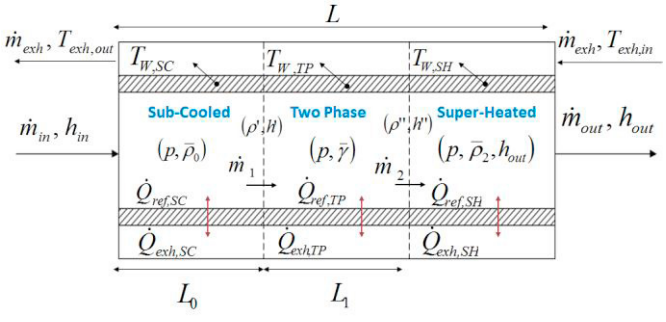

Fig. 3. Schematic and Notation for the Evaporator Model.

The equations for the complete evaporator model are obtained by applying (4) to each control volume, with reference to the schematic and notation summarized in Fig. 3. A detailed description the derivation procedure can be found in (Canova et al., 2015). The resulting set of equations is expressed in nonlinear descriptor form:

$$\Omega\left(x_{EV}\right)\cdot\frac{dx_{EV}}{dt} = b\left(x_{EV}, u_{EV}\right) \tag{5}$$

where the m-elements input and n-elements state variables arrays are:

$$u_{HEX} = \left[\dot{m}_{in} \quad \dot{m}_{out} \quad h_{in} \quad \dot{Q}_{SC} \quad \dot{Q}_{TP} \quad \dot{Q}_{SH}\right]^T \tag{6}$$

$$x_{HEX} = \left[L_0 \quad L_1 \quad p \quad h_{out} \quad \dot{m}_1 \quad \dot{m}_2\right]^T \tag{7}$$

The heat flux terms in (4) can be calculated through an additional lumped thermal mass model that characterizes the wall temperature dynamics and the heat transfer associated to the external and internal flows:

$$\frac{dT_{wall}}{dt} = \frac{\dot{Q}_{ext} - \dot{Q}_{\text{int}}}{C_{wall}} = \frac{\alpha_{ext}A_{ext}LMTD_{ext} - \alpha_{\text{int}}A_{\text{int}}\left(T_{wall} - T_{ref}\right)}{C_{wall}} \tag{8}$$

where C_{wall} (J/K) represents the heat capacity associated to the wall thermal mass. The heat transfer model accounts for internal and external convection, through appropriate correlations for the dimensionless heat transfer coefficients (Donowski et al., 2010).

The heat exchanger model presented above is based on the assumption that three different phase regions are always present in the heat evaporator. It is possible however that in some conditions the working fluid may enter or exit as a two phase fluid; this could happen, for instance, during start-ups or very fast transients. To deal with these cases, the original MBM has been modified by the authors to include a "switching" logic. The resulting switching MBM, presented in (Canova et al., 2015), adjusts the structure and number of states of the heat exchangers models to account for the presence or absence of a specific thermodynamic phase resulting from changes in the inlet and outlet conditions of the fluid.

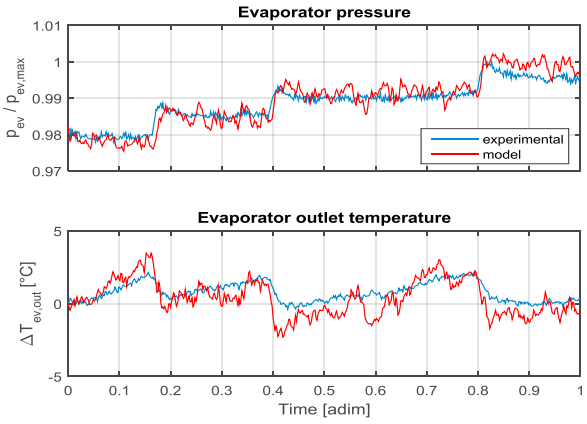

Fig. 4. Example of Transient Validation of the ORC Model.

Fig. 4 illustrates a comparison between model predictions and experimental data under step variations of pump speed.

3.5 Complete System

The complete ORC system model is obtained by connecting together the sub-models presented in the previous section, as depicted in Fig.5. The overall system model is expressed in nonlinear descriptor form, and includes 16 states, 3 controlled inputs and 3 exogenous inputs:

$$u_{ORC} = \begin{bmatrix} n_{pump} & x_{bp} & \dot{m}_{cool} \end{bmatrix}^T \tag{9}$$

$$\begin{aligned} x_{ORC} = \big[& L_{0,EV} \quad L_{1,EV} \quad p_{EV} \quad h_{EV,out} \quad T_{wallSC,EV} \\ & T_{wallTP,EV} \quad T_{wallSH,EV} \quad L_{0,COND} \quad L_{1,COND} \\ & p_{COND} \quad h_{COND,out} \quad T_{wallSC,COND} \quad T_{wallTP,COND} \\ & T_{wallSH,COND} \quad T_{REC,cold} \quad T_{REC,hot} \big]^T \end{aligned} \tag{10}$$

$$w_{ORC} = \begin{bmatrix} \dot{m}_{exh} & T_{exh} & n_{exp} \end{bmatrix}^T \tag{11}$$

In the rest of the paper it is assumed that the coolant mass flow rate is controlled through a PI controller to keep a condensing pressure of 2.5 *bar*. This reduces the number of control inputs to 2, namely the pump speed n_{pump} and the exhaust bypass x_{bp}.

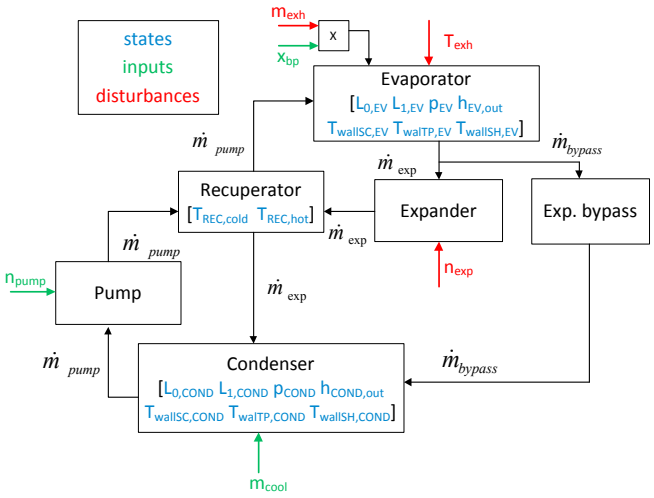

Fig. 5. Block Diagram of the Complete ORC Model.

4. TRANSIENT ANALYSIS

While ORC plants are typically designed to predominantly operate at steady-state conditions, where best performance can be achieved, (Briggs et al., 2010; Jensen, 2003), there is considerable interest in the automotive Industry to investigate the behaviour of the ORC system in presence of significant load transients.

To investigate the ability of the model to deal with transient conditions typical of automotive applications and to design a control policy able to properly deal with these situations, vehicle test data have been collected for an overtaking manoeuvre. A set of experimental data (including vehicle speed, exhaust gas temperature and mass flow rate, seen in Fig. 6, was collected on an instrumented vehicle equipped with a 2.0L turbocharged SI engine and a 6-speed manual transmission.

The specific manoeuvre, a common event during highway drive conditions, gives rise to significant variation in the heat flow through the evaporator, and represents an important test case for analysing the transient behaviour of the ORC system.

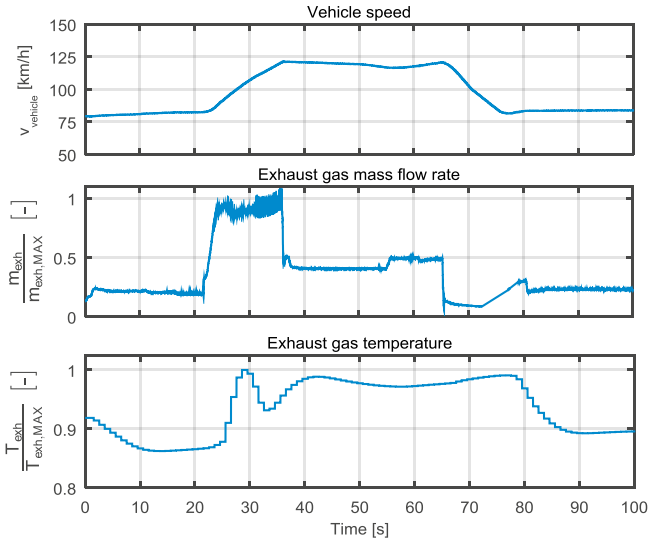

Fig. 6. Example of Acceleration/Deceleration Profile Measured on a Vehicle during an Overtaking Manoeuvre.

5. NONLINEAR MODEL PREDICTIVE CONTROL

To properly operate the ORC system in transient conditions, such as the one shown in Fig. 6**Error! Reference source not found.**, a suitable control policy has to be developed. The objective of the control design is to maximize the power output of the expander, namely the energy harvesting from the engine exhausts during the overall operation. At the same time, the controller should operate the ORC system safely, hence meet a set of state and input constraints. Classical optimal control methods (Kirk, 2012) applied to a complex nonlinear systems such as the ORC fail to produce a closed-form solution, or result computationally intractable. To this extent, a sub-optimal control strategy based on nonlinear model predictive control (NMPC) is proposed in this section.

This is intended as a "high level" control (similar to a supervisor in a hybrid vehicle), under the assumption that actuator-level feedback controllers are designed to track the desired inputs (i.e. bypass valve position and pump speed). This decentralized structure is common in many automotive control problems.

5.1 Sampled-Data Nonlinear MPC Problem Formulation

Consider a class of systems described by the following nonlinear differential equations:

$$\begin{aligned} \dot{x}(t) &= f(x(t), u(t), w(t)), \qquad x(0) = x_0 \\ y(t) &= h(x(t), u(t)) \end{aligned} \tag{12}$$

where $x(t) \in \mathbb{R}^n, u(t) \in \mathbb{R}^m, w(t) \in \mathbb{R}^s$ and $y(t) \in \mathbb{R}^p$ denote the vector of state, control input, exogenous signals and outputs, respectively. In (Canova et al., 2014), it was shown that the ORC system model in nonlinear descriptor

form (5) can be always converted into the explicit form (12) if the matrix $\Omega(x)$ is non-singular. This is guaranteed by the switching nature of the model.

It is assumed that the system is subject to input and output constraints of the form:

$$u(t) \in U := \{u \in \mathbb{R}^m | u_{min} \le u \le u_{max}\}$$
$$y(t) \in Y := \{y \in \mathbb{R}^p | y_{min} \le y \le y_{max}\}, \quad \forall t \ge 0 \tag{13}$$

The general NMPC problem is typically formulated as solving on-line a finite horizon open-loop optimal control problem subject to system dynamics and constraints as follows:

$$\min_{\bar{u}(\cdot)} J\left(x(t), \bar{u}(\cdot)\right) = E\left(\bar{x}(t+T_P)\right) + \int_t^{t+T_P} L\left(\bar{x}(\tau), \bar{u}(\tau)\right) d\tau \tag{14}$$
$$\begin{aligned} s.t. \quad & \dot{\bar{x}}(\tau) = f\left(\bar{x}(\tau), \bar{u}(\tau), \bar{w}(\tau)\right), && \bar{x}(t) = x(t) \\ & \bar{y}(\tau) = h\left(\bar{x}(\tau), \bar{u}(\tau)\right) \\ & \bar{u}(\tau) \in U, && \forall \tau \in [t, t+T_C] \\ & \bar{u}(\tau) = \bar{u}(t+T_C), && \forall \tau \in [t+T_C, t+T_P] \\ & \bar{y}(\tau) \in Y, && \forall \tau \in [t, t+T_P] \\ & \bar{x}(t+T_P) \in X_N \end{aligned}$$

where T_C and T_P denote the prediction and the control horizon with $T_C \le T_P$, and $L(\cdot,\cdot): \mathbb{R}^n \times \mathbb{R}^m \to \mathbb{R}$ and $E(\cdot): \mathbb{R}^n \to \mathbb{R}$ represent the state and terminal cost, and X_N the terminal constraint set. Moreover, note that $(\bar{x}(\tau), \bar{u}(\tau))$, denoted as the predicted system trajectories over the horizon $[t, t+T_p]$ starting from the initial condition $\bar{x}(t)$, are used to distinguish clearly from the real time system trajectories $(x(t), u(t))$. The solution of the problem (14) allows one to derive an open-loop optimal control law $\bar{u}^*(\cdot): [t, t+T_p] \to \mathbb{R}^m$ at time t, and such procedures, prediction and optimization, are then repeated in a receding horizon mechanism.

The primary objective in this study is to seek a numerical solution to the optimal control problem (14), which allows one to achieve the global minimal cost. In general, solving the control problem (14) in a continuous time representation (12) calls for the solution of a functional optimization problem. To this extent, a sampled-data structure (Magni and Scattolini, 2004; Findeisen et al., 2007) is instead considered in this study, where the manipulated control inputs are parameterized as piecewise constant signals during sampling intervals, i.e., $u(t) \equiv u(t_k) = const, \forall t \in [t_k, t_{k+1}), k \in \mathbb{N}$, where $\mathbb{N} := \{0,1,\dots\}$ and $t_k := kT$ with sampling period T.

Under such simplified formulation, the optimal control problem (14) could be effectively converted into a mathematical programming problem, which aims to find, at each sampling instance t_k, series of discretized control inputs of the form

$$\bar{\mathbf{u}}(t_k) = \left[\underbrace{\bar{u}_{0|t_k}, \bar{u}_{1|t_k}, \dots, \bar{u}_{N_C-1|t_k}}_{N_C}, \underbrace{\bar{u}_{N_C-1|t_k}, \dots, \bar{u}_{N_C-1|t_k}}_{N_P-N_C}\right] \tag{15}$$

where $\bar{u}_{j|t_k}, \forall j = 1, \dots, N_C - 1$ denotes the control vector at the j^{th} predicted step from the current sampling time t_k. In the following, the notation $\bar{u}_{j|t_k}$ will be simplified as $\bar{u}_j$ when it is clear from the context. Note that the first N_C vectors, which is a truncated control sequence as $\bar{u}_t(t_k) = [\bar{u}_0, \bar{u}_1, \dots \bar{u}_{N_C-1}]$, represent the optimization variables, and N_C, N_P represent the control and prediction steps such that $T_C = N_C T$ *and* $T_P = N_P T$. Finally, the first element from the optimized control policy is implemented into the ORC system as the finite horizon optimal control law:

$$u(t) := \bar{u}_0^*, \quad t \in [t_k, t_{k+1}) \tag{16}$$

5.2 Particle Swarm Receding Horizon Optimization

Since the optimal control problem (14) is non-convex, the usage of any convex optimization methods might lead to a non-optimal admissible solution. Therefore, it is crucial to find a generally applicable solution, robust optimization method able to handle the complex system dynamics of the ORC plant and the presence of state and input constraints. To this extent, a metaheuristic optimization method, based on the Particle Swarm Optimization (PSO), is proposed in this study to derive an optimal control input sequence under the framework of NMPC formulation described in previous section.

The PSO algorithm, originated from (Kennedy and Eberhart, 1995), is a stochastic, population based, gradient free and global optimization algorithm. The algorithm controls the motion of a swarm of particles within a defined search space, with each particle representing a potential solution to the optimization problem. The position and the velocity of each particle of the swarm are updated every iteration according to the algorithm as follows:

$$v_{j+1}^i = w v_j^i + r_1 c_1 \left(p_{best}^i - x_j^i\right) + r_2 c_2 \left(g_{best} - x_j^i\right) \tag{17a}$$
$$x_{j+1}^i = x_j^i + v_{j+1}^i, \qquad \forall i \in M, j = 1,2,\dots \tag{17b}$$

where the variables in equation (17) are summarized in Table 1. The first term in velocity equation (17a) represents the inertia term, which stores the particle velocity in the previous iteration and causes the particle to stray out of the general area of the swarm. The second and third terms in (17a) represent the cognitive and social components for the velocity update, respectively, where the former attracts each particle towards the best position held during its motion, while the latter attracts the particles towards the best position held by the swarm in its entirety, linking all particles together and sharing the experience of all the swarms. Terms c_1 and c_2 are weighting factors and r_1 and r_2 are stochastic factors that represent the source of randomness in algorithm.

Several variants of the PSO algorithm have been proposed to deal with constrained optimization problems. For instance, (Venter and Sobieszczanski-Sobieski, 2003) proposed to ignore the inertial term in the PSO velocity equation (17a) so that the unfeasible swarms can be steered back into the feasible region more effectively.

Table 1 Summary of Variables in the Particle Swarm Optimization Algorithm.

$M = \{1,2,\ldots,m\}$	particle population array
$v = [v_1, v_2, \ldots, v_m]$	particle velocity array
$x = [x_1, x_2, \ldots, x_m]$	particle location array
ω	inertia weight
p_{best}	personal best location
g_{best}	global best location
c_1	cognitive parameter
c_2	social parameter
r_1, r_2	stochastic factors in the range [0,1]
j	algorithm iteration

6. APPLICATION OF NMPC ON ORC SYSTEM FOR WASTE HEAT RECOVERY OPTIMIZATION

The goal of optimizing the ORC system for waste heat recovery equates into maximizing the energy recovered from the exhausts. The objective function is therefore expressed as a function of the net power produced by the ORC:

$$J = -\int_{t}^{t+N_p\Delta t} \left(P_{\exp} - P_{pump}\right) dt \tag{18}$$

The optimization problem needs to account for the physical constraints on the input variables (u_{min}, u_{max}), as the controls are physically bounded by the saturation limits. Moreover, the limits of variations rates of the actuators $(\dot{u}_{min}, \dot{u}_{max})$ should also be included. Other important limits include the safe operation of the system, such as the maximum pressure and temperature at the inlet of the expander, and a minimum amount of sub-cooling at the inlet of the evaporator. These conditions are treated as output constraints (y_{min}, y_{max}). Table 2 provides a summary of the system constraints. The limits were set according to recommendations from the BVG and expander suppliers.

Table 2 Summary of the ORC System Constraints.

Input constraints	
$50\ rpm \le n_{pump} \le 700\ rpm$	$0 \le x_{bp} \le 1$
Input rate of change constraints	
$\left\lvert \frac{dn_{pump}}{dt} \right\rvert \le 50\ rpm/s$	$\left\lvert \frac{dx_{bp}}{dt} \right\rvert \le 0.2\ x_{bp,\max}/s$
Output constraints	
$p_{ev} \le 30\ bar$	
$T_{ev,out} \le 180\ °C$	
$T_{ev,in} \le T_{sat} - 10\ °C$	

To apply the above algorithm, each particle describes a generic input sequence for the discretized optimization problem. Consequently, the search space of each particle has $N_c \times m$ dimensions. As the particles move through the search space during the execution of the algorithm, the cost function related to each different input sequence and the associated predicted state trajectory is evaluated for every particle at each iteration and then used to update the velocity, the personal and global best positions.

In particular, the formation of the finite horizon optimization problem with PSO allows one to directly handle the constraints on maximal input rate change by pre-screening the input sequence in each particle. Constraints for control inputs (u_{min}, u_{max}) and outputs (y_{min}, y_{max}) are handled within the PSO algorithm by maintaining the global best position inside the feasible region.

With an adopted population size of 100 particles, it is observed that within 15 iterations of the algorithm the swarm converges towards a solution for the optimization problem. Fig. 7 depicts the evolution of the pump speed trajectories evaluated in the receding horizon optimization at a given simulation time while the algorithm progresses and the particles of the swarm move toward the solution. In the first generation, the trajectories (each corresponding to a single particle) spread over the whole search space. Every trajectory starts from the same initial condition, and the stochastic terms $\Delta n_{pump}(k)$ are responsible for the generation of the different possible trajectories. As the algorithm progresses, the trajectories begin to overlap, indicating that the PSO algorithm converges to a solution and the particles of the swarm move towards the global best.

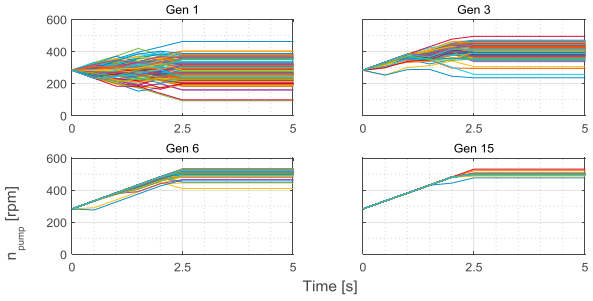

Fig. 7. Pump Speed Trajectories, PSO Generations 1, 3, 6, 15.

6. SIMULATION RESULTS AND ANALYSIS

The NMPC-PSO algorithm presented in the previous section is used to obtain the profiles of pump speed and bypass position; these trajectories are then applied to the same model used in the optimization to evaluate the performances. The results of the optimization are compared to those obtained from a basic feed-forward control policy, where the system was optimized at a large number of steady-state conditions, covering a range of possible operating points. For each point of the grid, the optimal steady-state control inputs for the ORC system were obtained by running the PSO algorithm (this time, however, as a simple static optimization at fixed exhaust gas conditions). Similar to the problem formulation for the NMPC, the feed-forward controller was obtained by optimizing the ORC system for maximum net power, under the same constraints presented in Table 1. Once the set of optimal steady-state control inputs is obtained, they are mapped in a lookup table as function of the exogenous inputs w_{ORC}, which are used to evaluate the corresponding set of control inputs during the transient.

Fig. 8 shows the resulting system net power for both the NMPC and the feed-forward control policies. The total power

at the expander is marginally higher during the load transient when using the simpler control policy. This however forces the ORC system to exceed the maximum evaporator pressure and superheat temperature. In fact, the feed-forward policy that results from the feasible solutions at steady state optimization has no mean of actively keeping the system inside the safe operating constraints during the transients. Since the dynamics of the ORC system are considerably slow compared to the engine, during the considered transient the ORC never reaches a steady state condition.

The NMPC algorithm, on the other hand, is able to properly maintain the system inside the safe operating region during the entire transient manoeuvre. This confirms the fact that a predictive algorithm, which explicitly accounts for the plant dynamics during the optimization process, should be used to properly control the ORC system.

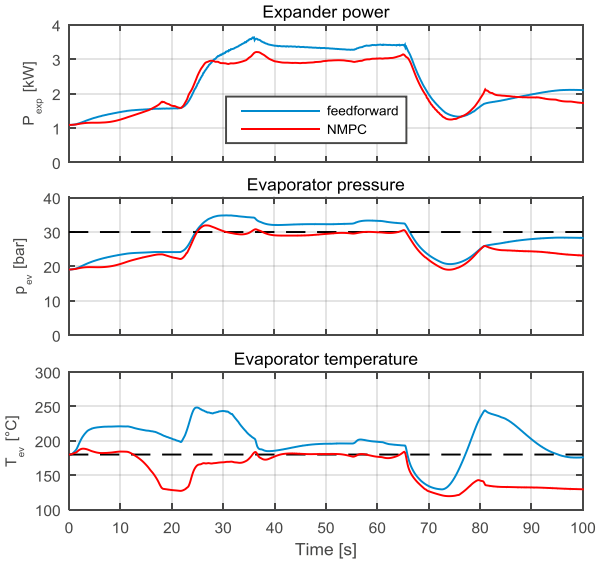

Fig. 8. ORC Net Power Output and System Constraints.

Furthermore, looking at the last 10 seconds of the transient, it appears that the feed-forward policy is able to grant a higher power output than the NMPC. This is however due to the fact that, with the feed-forward policy, the system is able to store a high amount of energy at the transient between 75 *s* and 85 *s*, when the maximum superheat temperature constraint is largely violated. After the load transient has ended, the exhaust gas energy decreases (as can be seen in Fig. 6), and the energy previously stored in the refrigerant by the feed-forward policy (when the constraints are violated) causes the slower decrease in the ORC performance.

Fig. 9 shows the optimal input profiles for both control policies. The bypass position is very similar in the two cases, except for the fact that the NMPC anticipates the feed-forward during the fast transients, thanks to the predictive ability of the algorithm. The main difference however lies in the pump speed, as the profile generated by the NMPC greatly differs from the one resulting from static optimization. Note that the pump speed target obtained from static optimization changes greatly during the transient, while the NMPC attempts to maintain it to a near-constant value, with only little fluctuations that help operating the system within the constraints.

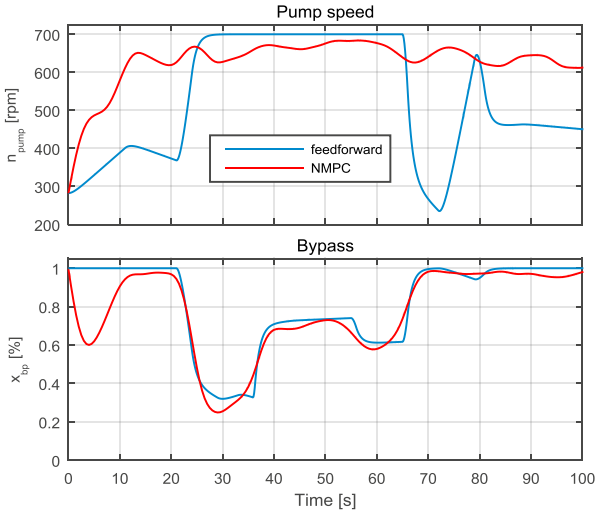

Fig. 9. Comparison of Controlled Input Profile for NMPC and Feed-Forward Strategies.

A pseudo-quality of the refrigerant at the outlet of the evaporator is depicted in Fig. 10. The pseudo-quality parameter χ allows for the distinction between different thermodynamic conditions:

$$\chi = \frac{h - h'}{h'' - h'} \tag{19}$$

where h' and h'' indicate the refrigerant enthalpy at the saturated liquid and saturate vapour states corresponding to the current pressure in the evaporator. While the parameter is in principle allowed to vary in the range $-\infty < \chi < +\infty$, a range $0 < \chi < 1$ indicates presence of a two-phase vapour in the system.

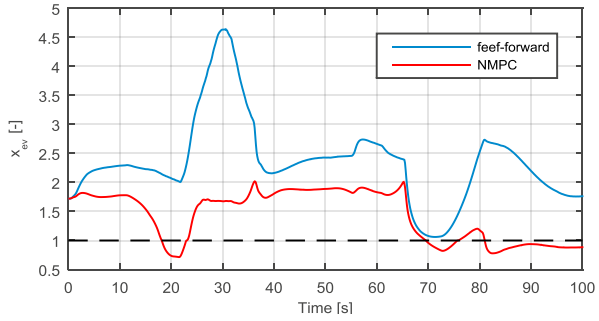

Fig. 10. Comparison of Evaporator Outlet Quality for NMPC and Feed-Forward Strategies.

As shown in Fig. 10, the NMPC algorithm operates the system such that two-phase vapour is present at the exit of the evaporator in two distinct conditions. The first event occurs at the beginning of the overtaking manoeuvre (from 18 *s* to 22 *s*), when the expander speed suddenly increases, while the second event occurs at the last part of the manoeuvre (from 75 *s* to 100 *s*), when the expander speed decreases again and there is not enough heat from the exhaust gases to fully vaporize the refrigerant. The same behaviour does not occur

with the feed-forward policy, due to the excess of heat absorbed by the system caused by the constraints violation.

Finally, improvements in fuel consumption given by the ORC system driven by the NMPC controller are estimated. The mass of fuel burned by the engine, considering the contribution of the ORC, is computed as:

$$m_{f,ORC} = \int_0^t \frac{P_{ICE} - P_{ORC}}{\eta_{ICE} \cdot LHV} \tag{20}$$

where P_{ORC} is the net power produced by the ORC.

With the above assumptions, the energy recovered by the ORC system during the acceleration-deceleration transient illustrated above results into a 6.2% reduction in the vehicle fuel consumption. The actual benefits in terms of FE will have to consider however other important factors that were not included in this study for simplicity, such as additional engine backpressure due to the BVG, weight increase, or additional fan power for removing heat from the condenser.

7. CONCLUSIONS

This paper presents a nonlinear model predictive control approach to optimize the transient response of an Organic Rankine Cycle for automotive exhaust waste heat recovery.

A high-fidelity, physics-based model was developed based on the Moving Boundary Method, and calibrated using components data from various suppliers. The model predicts the transient response of the condenser and evaporator heat exchangers, and includes a switching logic to avoid the model to become singular in presence of large variations in the controlled inputs and external disturbances.

A constrained optimal control problem is formulated with the objective of maximizing the net power output of the ORC system, while ensuring operations within the physical limits of the components. The problem is addressed by applying a nonlinear MPC, where the receding horizon optimization is based on a Particle Swarm Optimization (PSO) algorithm.

A verification of the NMPC-PSO solution was conducted considering a transient profile based upon experimental data collected on a test vehicle during an overtaking manoeuvre. The proposed control policy was compared to a feed-forward control, where the set-points for the ORC actuators were obtained by solving the same constrained optimization problem at several steady-state operating conditions. The simulation results demonstrate the effectiveness of the NMPC-PSO solution to operate the ORC system within its limits for the entire duration of the transient profile, while producing high net power output and reducing the thermal inertia of the system.

REFERENCES

Agarwal, N., Chiara, F., and Others (2012). Control-Oriented Modeling of an Auto-motive Thermal Management System, *Proc. of IFAC Workshop on Engine and Powertrain Control Simulation and Modeling (ECOSM), IFP Energies nouvelles, France*.

Canova, M., Crialesi Esposito, M., et al. (2014). Lumped-Parameter Modeling and Analysis of Automotive Waste Heat Recovery Systems Based on an Organic Rankine Cycle. *14th Stuttgart Int. Symposium,Stuttgart, Germany*.

Canova, M., Crialesi Esposito, M., and Others (2015). A switching Moving Boundary Method for the simulation of ORC plants in automotive applications. *15th Stuttgart International Symposium, ,Stuttgart, Germany* .

Chiara F., Canova M. (2013). A review of energy consumption, management, and recovery in automotive systems, with considerations of future trends. *Proc. Inst. Mech. Eng. Part D: J. Automobile Eng., 227(6), pp. 914–936.*

Donowski, V.D., Kandlikar, S.G., (2000). Correlating evaporation heat transfer coefficient of refrigerant R134a in a plate heat exchanger. *Proceedings of Boiling 2000 - Phenomena & emerging applications, Anchorage, Alaska.*

Edwards K.D., Wagner R., Briggs T. (2010). Investigating Potential Light-duty Efficiency Improvements through Simulation of Turbo-compounding and Waste-heat Recovery Systems. *SAE Paper 2010-01-2209.*

Feru, E., Willems, F., and Others (2014). Modeling and Control of a Parallel Waste Heat Recovery System for Euro-VI Heavy-Duty Diesel Engines. *Energies 7(10)*, pp. 6571-6592.

Findeisen, R., Raff, T., and Allgöwer, F. (2007). Sampleddata nonlinear model predictive control for constrained continuous time systems. *Advanced Strategies in Control Systems with Input and Output Constraints*, 207-235. Springer.

Jensen, J., (2003). Dynamic Modeling of Thermo-Fluid Systems. *PhD Dissertation*, Technical University of Denmark.

Kennedy, J., Eberhart R., (1995). Particle swarm optimization. *1995. Neural networks proceedings., IEEE International Conference, Perth, Australia*, volume (4), pp. 1942-1948.

Kirk, D. E. (2012). Optimal control theory: an introduction. Courier Corporation.

Lang W., Colonna P., Almbauer R. (2013). Assessment of Waste Heat Recovery From a Heavy-Duty Truck Engine by Means of an ORC Turbogenerator. *ASME J.of Eng.for Gas Turbines and Power, 135*.

Lemmon, E., McLinden, M., and Others (2007). *REFPROP: Reference fluid thermody-namic and transport properties*. NIST standard ref.database, 23(8.0).

Li B., Alleyne A., (2010). A dynamic model of a vapor compression cycle with shut-down and start-up operations. *International Journal of Refrigeration,* volume (33), pp. 538-552.

Magni, L. and Scattolini, R. (2004). Model predictive control of continuous-time nonlinear systems with piecewise constant control. *Automatic Control, IEEE Transactions on*, 49(6), 900-906.

McKinley T., Alleyne A., (2008). An advanced nonlinear switched heat exchanger model for vapor compression cycles using the moving-boundary method. *International Journal of Refrigeration*, volume (31), pp. 1253-1264

Mercieca, J., & Fabri, S. G. (2012). A metaheuristic particle swarm optimization approach to nonlinear model predictive control. *International Journal On Advances in Intelligent Systems*, 5(3 and 4), 357-369.

Peralez, J., Tona, P., and Others (2013). Improving the Control Performance of an Organic Rankine Cycle System for Waste Heat Recovery from a Heavy-Duty Diesel Engine using a Model-Based Approach. *52nd IEEE Conference on Decision and Control, Firenze, Italy.*

Sandou, G., & Olaru, S. (2009). Particle swarm optimization based nmpc: An application to district heating networks. In Nonlinear Model Predictive Control (pp. 551-559). Springer Berlin Heidelberg.

Seher D., Lengenfelder T., Gerhardt J., Eisenmenger N., Hackner M., Krinn I. (2012). Waste Heat Recovery for Commercial Vehicles with a Rankine Process. *21st Aachen Colloquium Automobile and Engine Technology, Aachen, Germany*.

Venter G., Sobieszczanski-Sobieski, J., (2003). Particle Swarm Optimization. *AIAA Journal*, volume (41), pp. 1583-1589.

Wang T., Zhang Y., Peng Z., Shu G., A review of researches on thermal exhaust heat recovery with Rankine cycle. *Renewable and Sustainable Energy Reviews*, 15, pp.2862–2871, 2011.